Submitted to QJRMS, August '97.

Accepted with minor mods. by QJRMS, Sept '97.

Resent December '97.

Air-Sea Fluxes Inferred from an Upper Ocean Heat Budget Northeast of the Azores.

M.E. McCulloch and H. Leach.

December 19, 1997

Summary.

The contributions to the seasonal heat budget of the upper 500 m of the North Atlantic between 33 and 60°N and 40 and 10°W were calculated using the Levitus and Boyer (1994) climatology and the Isemer and Hasse (1987) wind stress data. Near the Polar Front advection and diffusion were as important in the seasonal heat budget as the air-sea heat fluxes. In contrast, along a line extending between the Azores and the British Isles the air-sea heat fluxes were balanced primarily by heat content changes. Therefore, here, the air-sea fluxes could be inferred from the heat budget with an error of only 23 W m^{-2} because the large errors in estimates of the advection and diffusion were avoided. The inferred fluxes in this area were compared with the bulk formulae estimates of Isemer and Hasse (1987), Kent and Taylor (1995) and Josey *et al.* (1996) and agreed most closely with the latter.

1 Introduction.

(a) Overview.

The flux of heat between the air and the sea Q_H can be written as

$$Q_H = Q_{SW} + Q_{LW} + Q_{LA} + Q_{SE} \tag{1}$$

where Q_{SW} is shortwave heat radiation, Q_{LW} represents air–sea longwave heat exchange and Q_{LA} and Q_{SE} are the latent (evaporative) and sensible (conducted) heat fluxes. The last two processes can be parameterized using the semi-empirical bulk formulae

$$Q_{LA} = L\rho C_E \; U(q_{SS} - q_{10}) \tag{2}$$

$$Q_{SE} = c_p \rho C_H \; U(T_{SS} - T_{10}) \tag{3}$$

where L is the latent heat of vapourisation, ρ is air density, q_{SS} and q_{10} are the humidities at the sea surface and 10 m height respectively, c_p is the specific heat capacity of water at constant pressure, T_{SS} and T_{10} are the air temperature at the sea surface and 10 m height and U is the wind speed.

The bulk transfer coefficients C_E and C_H depend on wind speed and errors associated with them (15% according to Smith *et al.*, 1995) contribute largely to the uncertainty in the total air-sea flux which may be as large as 30 W m^{-2} (Isemer and Hasse, 1987). This error was deduced from differences between the area–integrated annual air–sea heat flux in the North Atlantic and observations of northward oceanic heat transports (Isemer *et al.*, 1989) and is therefore a systematic error. It implies that if the fluxes are used as a boundary condition for ocean or atmosphere models the errors in temperature incurred after three months are 1 K (for the ocean mixed layer) and 25 K (for the troposphere). This indicates why relaxation boundary conditions are widely used in such models. The error in the fluxes is also an order of magnitude larger than changes in the flux that would occur due to doubling atmospheric CO_2 concentrations (Houghton *et al.*, 1990) and so contributes to uncertainty in long-term climate studies. Therefore, improved accuracy in the fluxes would be useful.

To choose the best of the available bulk formula flux climatologies we can compare their fluxes with the fluxes calculated, independent of the bulk formulae, using the heat budget method. In this method the fluxes are inferred from differences between the observed heat content change and estimates of heat advection and diffusion. Behringer and Stommel (1981) used this approach in the tropical Atlantic, and Pransgma *et al.* (1983) in the northern North Atlantic, for example. One problem with this technique is that estimates of advection and diffusion can introduce large errors into the inferred fluxes. Garrett *et al.* (1993) eliminated this problem by considering the Mediterranean, a closed basin from which the advection and diffusion of heat are small.

Here, a study of the ocean heat budget shows that between the Azores and the British Isles, advection and diffusion contribute little to the seasonal heat budget. Therefore, in this area, as in Garrett *et al.* (1993) the air-sea heat fluxes can be inferred with minimum error and compared with recent climatological estimates.

(b) The Heat Budget.

The Eulerian rate of change of temperature (T) in the ocean can be written as

$$\frac{\partial T}{\partial t} = \frac{1}{\rho c_p}\frac{\partial Q_H}{\partial z} - (\underline{u}_g + \underline{u}_e).\nabla T - w_e\frac{\partial T}{\partial z} + K_h \nabla^2 T + K_v \frac{\partial^2 T}{\partial z^2} \qquad (4)$$

where ρ and c_p are the density and specific heat capacity of sea water, Q_H represents the vertical diabatic heat flux, u and w are the horizontal and vertical components of the flow, where the subscripts g and e represent the geostrophic and Ekman components. K_h and K_v are the horizontal and vertical diffusion coefficients respectively. Thus, term 1 on the right hand side is the diabatic heat flux, terms 2 and 3 are geostrophic and Ekman advection of heat, term 4 is vertical advection by Ekman pumping and terms 5 and 6 are horizontal and vertical diffusion. We integrate (4) from a depth L to the ocean surface. In order to include the entire seasonal thermocline, which in the Northeast Atlantic is unusually deep in winter, L was chosen as 500 m. We assume that the vertical diabatic heat flux and the vertical flow are zero at depth L and the heat content (H) of the upper 500 m is given by

$$H = \rho c_p \int_{-L}^{0} T(z)\, \mathrm{d}z \qquad (5)$$

Using (4) and (5) we obtain an expression for the rate of heat content change for a water column of unit area

$$\frac{\partial H}{\partial t} = Q_H + \rho c_p \int_{-L}^{0} \left(-(\underline{u}_g + \underline{u}_e).\nabla T - w_e \frac{\partial T}{\partial z} + K_h \nabla^2 T + K_v \frac{\partial^2 T}{\partial z^2} \right) \mathrm{d}z \qquad (6)$$

In this paper the first term on the right, the air-sea heat flux Q_H is quantified seasonally by calculating all the other terms for the seasons of winter (DJF, ie: December–February), spring (MAM), summer (JJA) and autumn (SON).

2 Method.

(a) The Levitus Atlas Data.

For this analysis the Levitus and Boyer (1994) World Ocean Atlas data between 33 and 60°N and 10 and 40°W were spatially averaged over squares with sides of length 3° north–south and 300 km east–west in order to eliminate eddy–scale variations. Figure 1 shows (by crosses) the centres of these squares and also, to give some idea of the hydrography of the area, the contours show the March sea surface temperature. The North Atlantic Polar Front can be seen in the northwest, indicated by the close spacing of the isotherms and represents the boundary between, to the north, cold and fresh sub–polar water and in the south the saline and warmer North Atlantic Central Water. The Levitus data were used to produce average temperature and salinity profiles for each square. The contributions of each process in equation 6 (discussed in more detail below) were calculated monthly for each depth level available in the Levitus Atlas above 500 m depth, summed over that depth and then averaged over each season. The seasonal rate of change of heat content for each square was calculated by differencing the average temperature profiles at the beginning and end of each season.

(b) Geostrophic Advection.

The baroclinic component of the geostrophic flow ($\underline{u}_g$) was calculated using density profiles for the 3° squares derived from the Levitus annually-averaged temperatures and salinities using the Dynamic method:

$$\underline{u}_g(z) = \frac{g}{\rho f} \int_{-Z}^{z} \hat{\underline{k}} \times \underline{\nabla} \rho \, \mathrm{d}z, \tag{7}$$

where $\underline{u}_g(z)$ is the flow at depth z, f is the Coriolis parameter, $\underline{\hat{k}}$ is a unit vertical vector and the level of no motion (Z) was taken as 1500 m. The various assumptions made in this paper (eg: the value for Z) were tested in a sensitivity study (see section 3a for a discussion). The flow calculated at each depth was applied to the horizontal gradient in heat content at that depth, calculated by centred–differencing, and the results summed over 500 m. Figure 2 shows the annual average surface geostrophic flow (vectors) and geostrophic heat advection (contours). The flow was maximum (5 cm s^{-1} eastwards) at 51^{o}N, 35^{o}W in the North Atlantic Current (NAC). Further south, where the flow was directed at a greater angle with respect to the isotherms, it caused a heat content increase of up to 80 W m^{-2}. There was a heat content decrease of 40 W m^{-2} west of Portugal due to the slow southward flow there. Along a line between the Azores (39^{o}N, 29^{o}W) and the British Isles the geostrophic heat advection was less than 20 W m^{-2}. For comparison Paillet and Arhan (1996) estimated that the (baroclinic) geostrophic heat advection in this area (along 20^{o}W) for a column 600 m deep was 4 W m^{-2}.

(c) Ekman Processes.

The average wind stress for each season was obtained from the revised Bunker Atlas (Isemer and Hasse, 1987) and spatially averaged for each 3^o square. Since only the vertical integral of the Ekman flow, the Ekman transport ($\mathbf{U}_e$) is calculable from the wind stress (τ) as

$$\underline{\mathbf{U}}_e = -\frac{\underline{\hat{k}} \times \underline{\tau}}{f} \tag{8}$$

and the third term in Eq. 6 was modified thus

$$\rho c_p \int_{-L}^{0} \underline{u}_e.\nabla T \, \mathrm{d}z \;=\; \rho c_p (\underline{\mathbf{U}}_e.\nabla T_e) \qquad (9)$$

where T_e was the average temperature in the Ekman layer. The Ekman layer depth, which itself varies with the wind stress, was calculated monthly and (between the Azores and the British Isles) it varied only between 30 in summer and 50 m in winter. A constant Ekman depth of 40 m was therefore chosen for the determination of T_e.

Figure 3 shows the annual average Ekman transport (vectors) and Ekman heat advection (contours). The transport was directed southward over the Polar Front, due to prevailing westerly winds, causing a heat content decrease of up to 60 W m^{-2}. Despite the fact that the Ekman flow was restricted to the upper 40 m and the geostrophic flow extended to 500 m, the Ekman advection was as important as geostrophic advection. This was because the Ekman flow was directed perpendicular to isotherms whereas the geostrophic flow, because of its dependence on density variations, is usually aligned roughly *along* the isotherms. However, the Ekman heat advection was smaller between the Azores and the British Isles.

The Ekman pumping speed was obtained for each season from the Bunker Atlas, averaged for each 3^o square, taken as the vertical velocity at the Ekman depth (40 m) and assumed to decay linearly to zero at the surface and 500 m depth. Figure 4 shows the annual average contribution of Ekman pumping to the heat budget (contours). There was a heat content increase near the Azores because of the anticyclonic (high pressure) wind system centred there, which caused horizontal Ekman convergence and a downwelling of summer–warmed surface water. This effect showed a seasonal cycle (see Fig. 7) and was greatest in autumn when the vertical temperature gradients were maximum.

(d) Diffusion.

The horizontal (eddy) and vertical diffusion were calculated for each month and square using horizontal and vertical diffusion coefficients of 5000 m^2s^{-1} (after Schäfer and Krauss, 1995) and 2×10^{-5} m^2s^{-1} (the diapycnal diffusion coefficient determined by Ledwell *et al.*, 1993) respectively. Figure 5 shows the combined contribution of vertical and horizontal diffusion to the heat budget. There was a heat content decrease at 46°N, 38°W south of the Polar Front as the relatively warm waters of the NAC lost heat northwards across the Front, but vertical diffusion had little effect. Away from the Front the effects of diffusion were small.

3 Results.

(a) Minimizing Errors in The Heat Budget.

Figure 6 shows (by contours) the combined contribution of advection and diffusion to the annual average heat budget of the upper 500 m across the Northeast Atlantic. In a sensitivity study the parameters used in the analysis (see Table 1, column 2) were varied by their assumed uncertainty (see Table 1, column 3) and the effect on the predicted heat content change of Fig. 6 (heat advection and diffusion) was determined. In this study the geostrophic level of no motion was varied by 500 m (see Table 1, row 1) as estimates of this depth vary between 1 and 2 km. A barotropic flow equal to 10 % of the local geostrophic flow was also added in a direction perpendicular to the isotherms (northwards) to have the largest effect on the heat budget (row 2). The errors in Ekman advection and Ekman pumping were determined assuming a $\pm$ 3 m s^{-1} random error in wind stress (Lindau, 1994) (row 3). The error in the horizontal and vertical diffusion coefficients (K_h and K_v) were taken as 100 % since the values are not well known (rows 4 and 5). Estimates of K_h for example, vary widely between 1×10^3 and 10×10^3 m^2 s^{-1}. The standard error in the temperature values was determined from the standard deviations (over 5^o boxes) given in the Levitus Atlas (row 6).

Near the NAC the contributions of advection and diffusion to the heat budget were large (Fig. 6) and the errors were over 100 W m^{-2}. Therefore the fluxes inferred here included large errors. In this area geostrophic and Ekman advection and eddy diffusion were each as important in the seasonal heat budget of the upper 500 m as the air-sea heat fluxes.

However, for six squares located between the Azores and the British Isles (circled in Fig. 6) advection and diffusion combined contributed only 20 W m^{-2} to the heat budget and the errors were less than $\pm$ 10 W m^{-2}. Table 1, column 4 summarizes the results of the sensitivity study for these six squares. The total error in the air-sea heat fluxes inferred from the heat budget (Table 1, row 8) was smaller, at 23 W m^{-2}, than the $\sim$ 30 W m^{-2} errors in bulk formula estimates, and was primarily determined by errors in the observed heat storage (Table 1, row 6). Therefore, to improve the fluxes inferred from the heat budget it would be most useful, in this area, to improve the observations of heat content change, and highly accurate knowledge of the flow or temperature gradients is less important.

Figure 7 shows the observed heat content change, and the contribution of each process in Eq. 6 to that change, averaged over each season and the six squares circled in Fig. 6. The rate of heat content change reached +90 W m^{-2} in summer and -75 W m^{-2} in winter. However, the contributions of advection and diffusion were far too small to account for the seasonal heat content changes. The most important processes were Ekman advection which caused a heat content decrease of up to 18 W m^{-2} in winter (when the wind stress was greatest) due to southward flow, and Ekman pumping which caused a heat content increase up to 17 W m^{-2} in summer and autumn when the seasonal thermocline was most developed.

(b) Comparison of Air-Sea Heat Fluxes.

Figure 8 (thick line) shows the air-sea heat flux required to balance the heat budget shown in Fig. 7 with error bars of 23 W m^{-2} (see Table 1). Various bulk formulae estimates of the air-sea heat fluxes (see Table 2 for their errors) are also shown.

The air-sea heat fluxes estimated by Isemer and Hasse (1987) (referred to as IH hereafter) are shown in Fig. 8 by a thin line. According to Kent and Taylor (1995) these fluxes include better estimates of the latent and sensible heat fluxes than other contemporary climatologies and in this case they agreed well with the heat budget fluxes in the summer. However, the IH fluxes showed a much larger (by 60 W m^{-2}) loss of heat by the ocean in winter and autumn. The fluxes inferred from the heat budget were compared quantitatively with the bulk formulae estimates by summing the modulus of the difference between the two fluxes over the four seasons, then dividing by four. This "average difference" between the IH fluxes and the heat budget fluxes was 34 W m^{-2} (see Table 2, column 3).

Kent and Taylor (1995) (hereafter KT) concluded that, although the IH fluxes were more successful than other estimates, IH's latent and sensible heat transfer coefficients were too large. This conclusion agrees with the results in Fig. 8 where the IH fluxes overestimate the ocean's heat loss in winter compared with the heat budget fluxes. Isemer and Hasse (1987) had increased their latent and sensible heat fluxes to enhance the loss of heat by the ocean in the northern North Atlantic so that classical estimates of the northward heat transport in the Atlantic would agree with direct estimates from zonal hydrographic sections (Isemer *et al.*, 1989). KT disagreed with this increase in ocean heat loss and suggested that the IH latent and sensible heat fluxes should be reduced as follows

$$Q_{LA} = 0.72 \times Q_{LA} + 12.5 \tag{10}$$

$$Q_{SE} = 0.63 \times Q_{SE} + 2.4 \tag{11}$$

The thin dashed line in Fig. 8 shows the IH fluxes revised in this way and renamed the KT fluxes. The KT fluxes agreed much better with the heat budget fluxes in winter and autumn but the difference was increased in the spring and summer. Over the four seasons, however, the average difference was reduced from 34 to 26 W m^{-2} (see Table 2).

The IH and KT fluxes were calculated using the Bunker Atlas data set (Bunker, 1976) which included 7 million observations collected between 1941 and 1972. These fluxes may be biased by changes in the methods of observation of the wind stress over this period (Garrett *et al.*, 1993) and also by interdecadal variability. Also shown in Fig. 8 are two flux estimates of Josey *et al.* (1996) (referred to as JKOT) which were calculated using the COADS 1a data set instead of the Bunker data. The COADS 1a data was based on 30 million observations from the (shorter) period between 1980 and 1993. As well as relying on a better data set the versions of the bulk formulae used by JKOT were supported by more recent data, and were altered to correct for observational biases in ship data determined from the WMO47 list of ships. The fluxes of JKOT are also shown in Fig. 8 and agreed with the heat budget fluxes better than the IH or KT fluxes. The average difference was reduced from 26 to 22 W m^{-2} (see Table 2).

Josey *et al.* (1996) later increased their ocean latent heat losses by 10 % to account for biases due to dirt on the wicks of wet-bulb thermometers. A further aerosol–loading correction to the fluxes was also applied south of 30^{o}N (not relevant here). The revised JKOT fluxes in this case were only slightly different from the original JKOT fluxes (see Table 2).

Therefore, both the JKOT fluxes were more successful than those of IH and KT. To achieve a more conclusive comparison between the two JKOT flux fields it would be useful to perform a similar analysis south of 30^{o}N where the aerosol correction should be significant.

(c) Annual Air-Sea Heat Fluxes.

Table 2 (column 2) shows the annual average air-sea heat flux (for the usual six squares) as inferred from the heat budget (row one) and for comparison the annual flux estimated using the various bulk formulae estimates. The errors (in brackets) were determined, in the cases of the Isemer and Hasse fluxes by Isemer *et al.* (1989) as 30 W m^{-2} (a bias) and in the other cases by adding together 20 % of each (annual average) flux component in quadrature as suggested by Hsiung (1986). The original JKOT fluxes shown on row 4 agreed most closely with the fluxes derived from the heat budget, although all the estimates agreed within their error bars. The large scatter of 46 W m^{-2} shows the uncertainty that still exists in recent air-sea flux estimates, even in an area which is well covered by ship surveys.

4 Conclusions.

The contributions to the seasonal heat budget of the upper 500 m of the Northeast Atlantic were calculated using the Levitus and Boyer (1994) climatology. Near the Polar Front heat advection and diffusion were as important in the seasonal heat budget as the air–sea heat fluxes. In contrast, between the Azores and the British Isles, the air–sea heat fluxes were balanced primarily by heat content changes. Therefore, here, it was only errors in the observed heat content changes that limited the accuracy to which air–sea fluxes could be inferred from the heat budget, and not the usually larger errors in estimates of advection or diffusion. The air–sea heat fluxes were inferred here with errors of only $\pm$ 23 W m^{-2}. The inferred fluxes were compared with the bulk formula estimates of Isemer and Hasse (1987), Kent and Taylor (1995) and Josey *et al.* (1996) and agreed most closely with the latter.

Acknowledgements.

Many thanks to R.G. Williams and K. Stratford for advice. This work was funded by NERC's UK WOCE program.

References.

Behringer, D.W. and H. Stommel, 1981. Annual heat gain of the tropical Atlantic computed from sub-surface ocean data. *JPO*, **11**, 1393-1398.

Bunker, A.F. 1976. Computations of surface energy flux and annual air-sea interaction cycles of the North Atlantic ocean. *Mon. Wea. Rev.*, **104**, 1122-1140.

Garrett, C., R. Outerbridge and K. Thompson, 1993. Interannual variability in mediterranean heat and buoyancy fluxes. *J. Climate*, **6**, 900-910.

Houghton, J.T., G.J. Jenkins and J.J. Ephraums., 1990. Climate change. The IPCC scientific assesment. Cambridge University Press.

Hsiung, J., 1986. Mean surface energy fluxes over the global ocean. J. Geophys. Res., Volume 91, Number C9, 10585-10606.

Isemer, H-J. and L. Hasse, 1987. The Bunker Climate Atlas of the North Atlantic Ocean. Vol. 2: Air-Sea Interaction. Report no. 160a of the Institut für Meereskunde, Christian-Albrechts Universität, Springer-Verlag.

Isemer, H-J., J. Willebrand and L. Hasse, 1989. Fine adjustment of large scale air-sea energy flux parameterizations by direct estimates of ocean heat transport. *J. Climate*, **2**, 1173-1184.

Josey, S.A., E.C. Kent, D. Oakley and P.K. Taylor, 1996. A new global air-sea heat and momentum flux climatology. *International WOCE Newsletter*, **24**, 3-5.

Kent, E.C. and P.K. Taylor, 1995. A comparison of sensible and latent heat flux estimates for the North Atlantic ocean. *J. Phys. Oceanogr.*, **25**, 1530-

1549.

Ledwell, J.R., A.J. Watson, C.S. Law, 1993. Evidence for slow mixing across the pycnocline from an open–ocean tracer release experiment. *Nature*, **364**, 701-703.

Levitus, S. and T.P. Boyer, 1994. World Ocean Atlas 1994. U.S Department of Commerce, Washington D.C.

Lindau ,R., 1994. Eine neue Beaufort Äquivalentskala. *Ber. Inst. Meeresk.*. Kiel, **249**, 134 pp.

Marshall, J.C., A.J.G. Nurser and R.G. Williams, 1993. Inferring the subduction rate and period over the North Atlantic. J. Phys.Oceanogr., Volume 23, 1315-1329.

Paillet, J and M. Arhan, 1996. Shallow pycnoclines and mode water subduction in the eastern North Atlantic. *J. Phys. Oceanogr.*, **26**, 96-114.

Prangsma, G.J., T.H. Guymer, P. Kruseman, R.T. Pollard and R.A. Weller, 1983. Development of temperature and salinity structure of the upper ocean over two months in an area 150 × 150 km. *Phil. Trans. R. Soc. Lond. A.*, **308**, 311-325.

Schäfer, H. and W. Krauss, 1995. Eddy statistics in the South Atlantic as derived from drifters drogued at 100 m. *J. Mar. Res.*,**53**, No. 3, 403–431.

Smith, S.D., C.W. Fairall, G.L. Geernaert, L. Hasse, 1995. Air–sea fluxes: 25 years of progress. *Boundary – –layer meteorology*,**78**, No. 3-4, 247–290.

Captions.

Figure 1. Map showing the centres (crosses) of the squares over which the Levitus Atlas data was averaged and the March sea surface temperature (°C).

Figure 2. The vectors show the surface geostrophic flow (cm s^{-1}) calculated using the dynamic method and the contours show the geostrophic advection of heat (W m^{-2}) in the upper 500 m.

Figure 3. The vectors show the annual average Ekman transport (m^{-2} s^{-1}) and the contours show the annual Ekman advection of heat (W m^{-2}).

Figure 4. The contours show the annual average Ekman pumping of heat (W m^{-2}) in the upper 500 m.

Figure 5. The contours show the annual average horizontal and vertical diffusion of heat (W m^{-2}) in the upper 500 m.

Figure 6. The contours show the annual average heat content change (W m^{-2}) due to Ekman and geostrophic advection, Ekman pumping and diffusion in the upper 500 m and the bold numbers show the errors.

Figure 7. The seasonal heat budget (W m^{-2}) for six squares between the Azores and the British Isles showing the heat content change, and the contribution of each process in the heat budget (except the air–sea fluxes).

Figure 8. The seasonal air–sea heat fluxes (W m^{-2}) inferred from the heat budget of Fig. 7, and as estimated by recent climatologies.

SENSITIVITY STUDY ON THE HEAT BUDGET

Error due to	Parameter	Error	Error in Q_H
geostrophic advection	Z	$\pm$ 500 m	$\pm$ 3
	u_g	$\pm$ 0.2 cm s^{-1}	$\pm$ 8
Ekman advection	wind speed	$\pm$ 3 m s^{-1}	$\pm$ 3
Ekman pumping			$\pm$ 4
horiz. diffusion	K_h	$\pm$5000 m^2 s^{-1}	$\pm$ 3
vert. diffusion	K_v	100 %	$\pm$ 7
dH/dt	T	$\pm$ 0.2 K	$\pm$19
Root–sum–square			$\pm$23

Table 1: Results of a sensitivity study showing how uncertainties (column 3) in various parameters (column 2) used in the heat budget calculation effected the inferred average air-sea heat flux Q_H (column 4, W m^{-2}) for six squares between the Azores and the British Isles.

COMPARISON BETWEEN AIR–SEA HEAT FLUX ESTIMATES

Estimate of Q_H	Annual flux (W m^{-2})	Difference (W m^{-2})
From heat budget	10 ($\pm$ 23)	0
Isemer and Hasse (1987)	-12 (30)	34
Kent and Taylor (1995)	34 ($\pm$ 33)	26
Josey *et al.* (1996) (orig.)	11 ($\pm$ 32)	22
Josey *et al.* (1996) (revd.)	-2 ($\pm$ 33)	21

Table 2: The net annual air-sea heat flux from various sources (W m^{-2}) and errors (in brackets) for six squares between the Azores and the British Isles. Column 3 shows the mean seasonal difference between each bulk formulae estimate and the heat budget estimate.

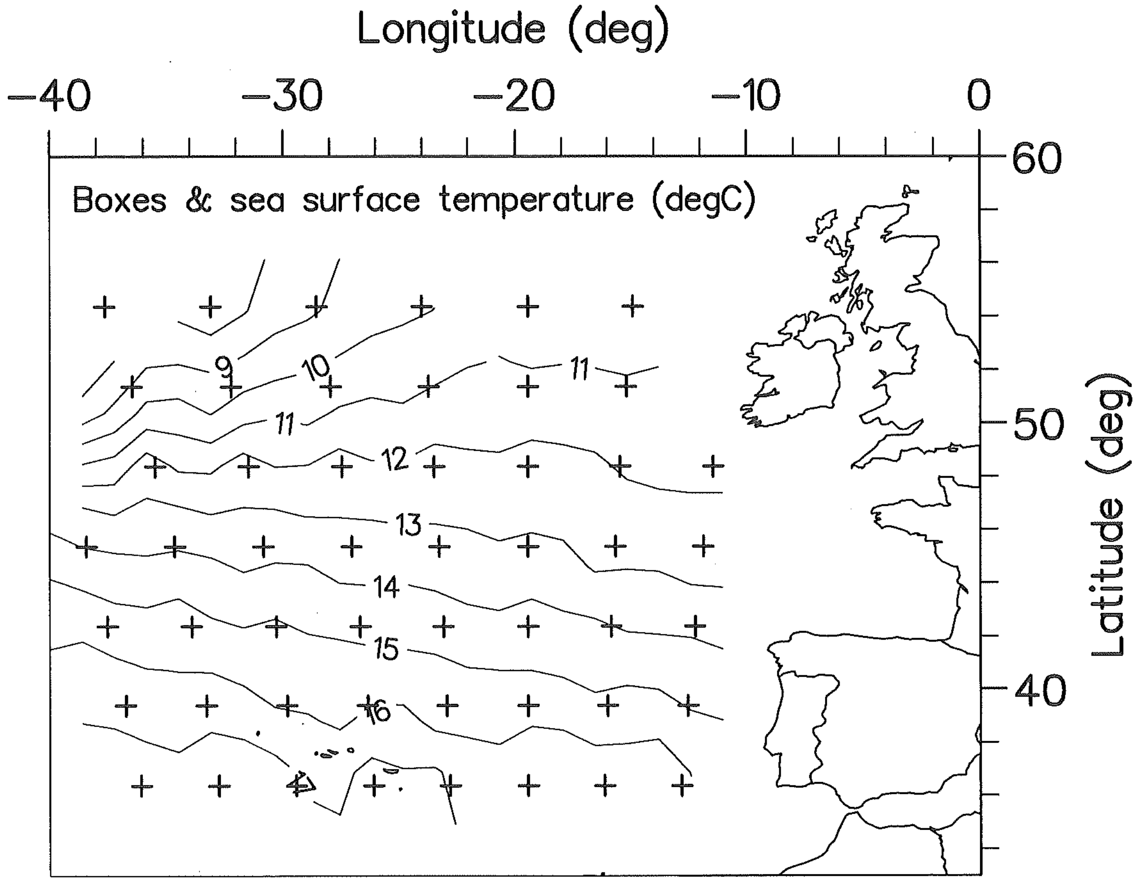

Longitude (deg)
−40
−30
−20
−10
0
60
50
40
Latitude (deg)
Boxes & sea surface temperature (degC)
9
10
11
11
12
13
14
15
16
17

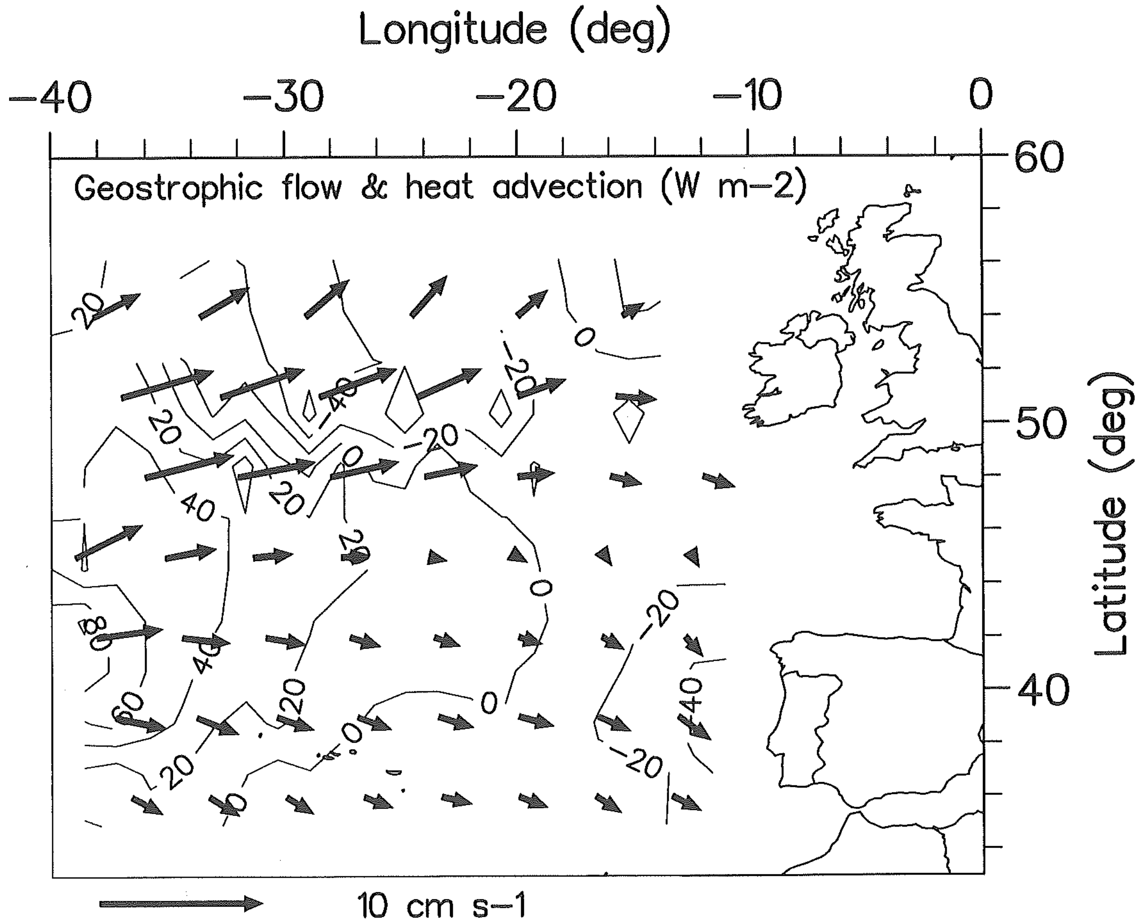

Longitude (deg)
−40
−30
−20
−10
0
60
50
40
Latitude (deg)
Geostrophic flow & heat advection (W m−2)
10 cm s−1

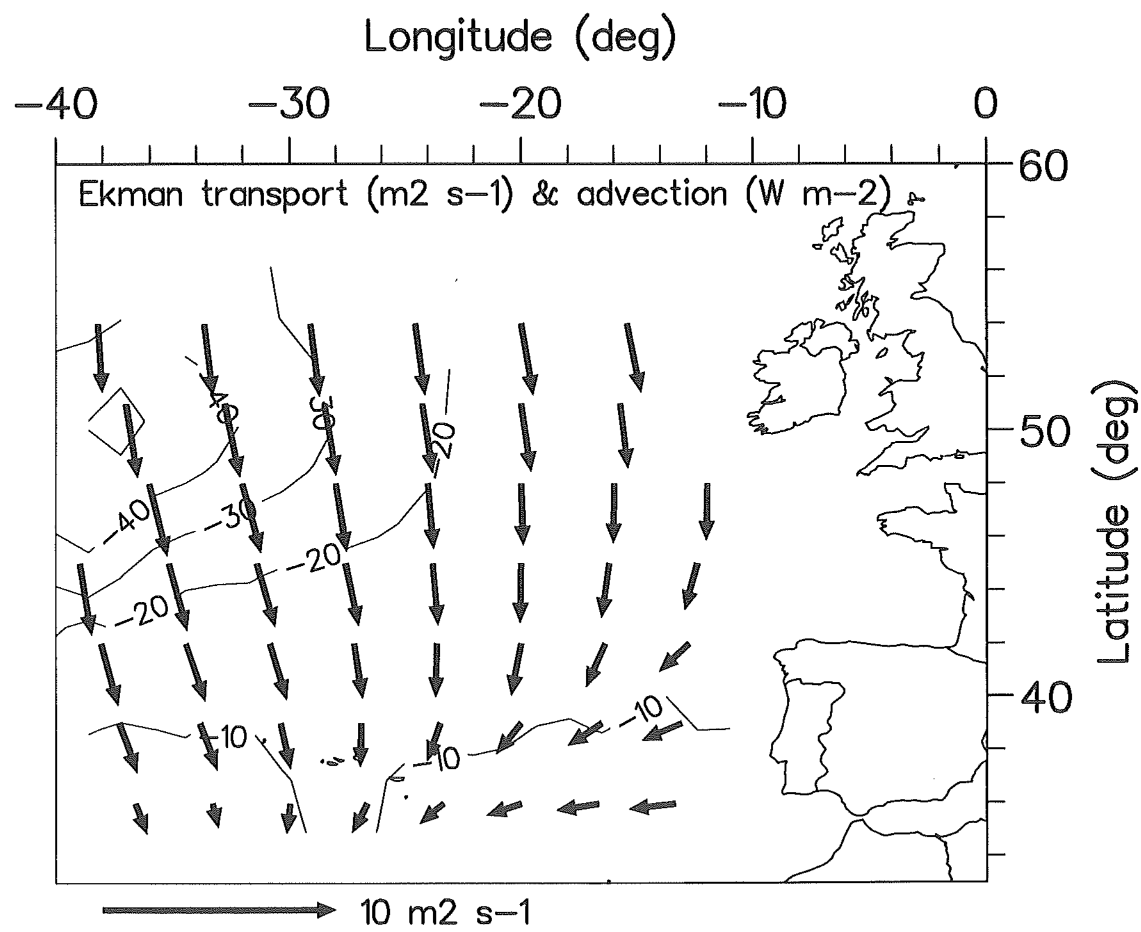
Longitude (deg)
−40
−30
−20
−10
0
60
50
40
Latitude (deg)
Ekman transport (m2 s−1) & advection (W m−2)
−40
−30
−20
−10
10 m2 s−1

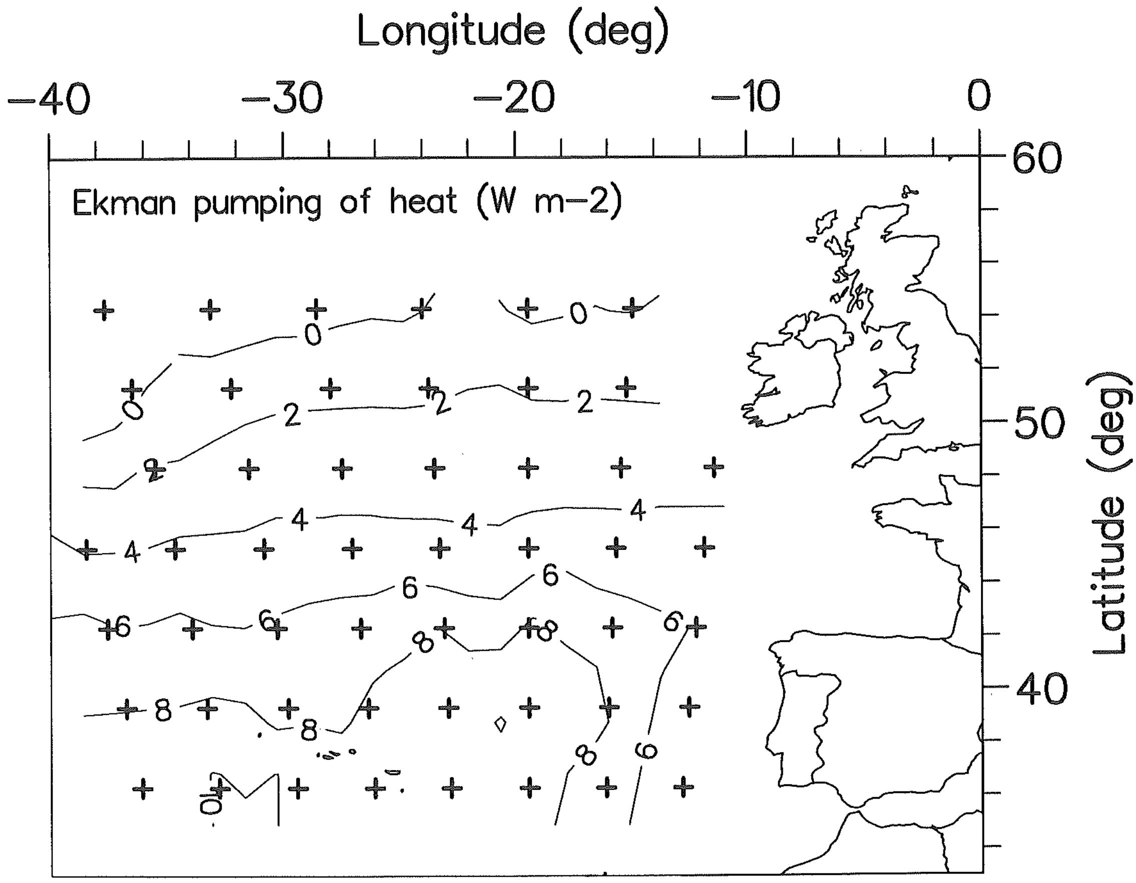
Longitude (deg)
−40
−30
−20
−10
0
60
50
40
Latitude (deg)
Ekman pumping of heat (W m−2)

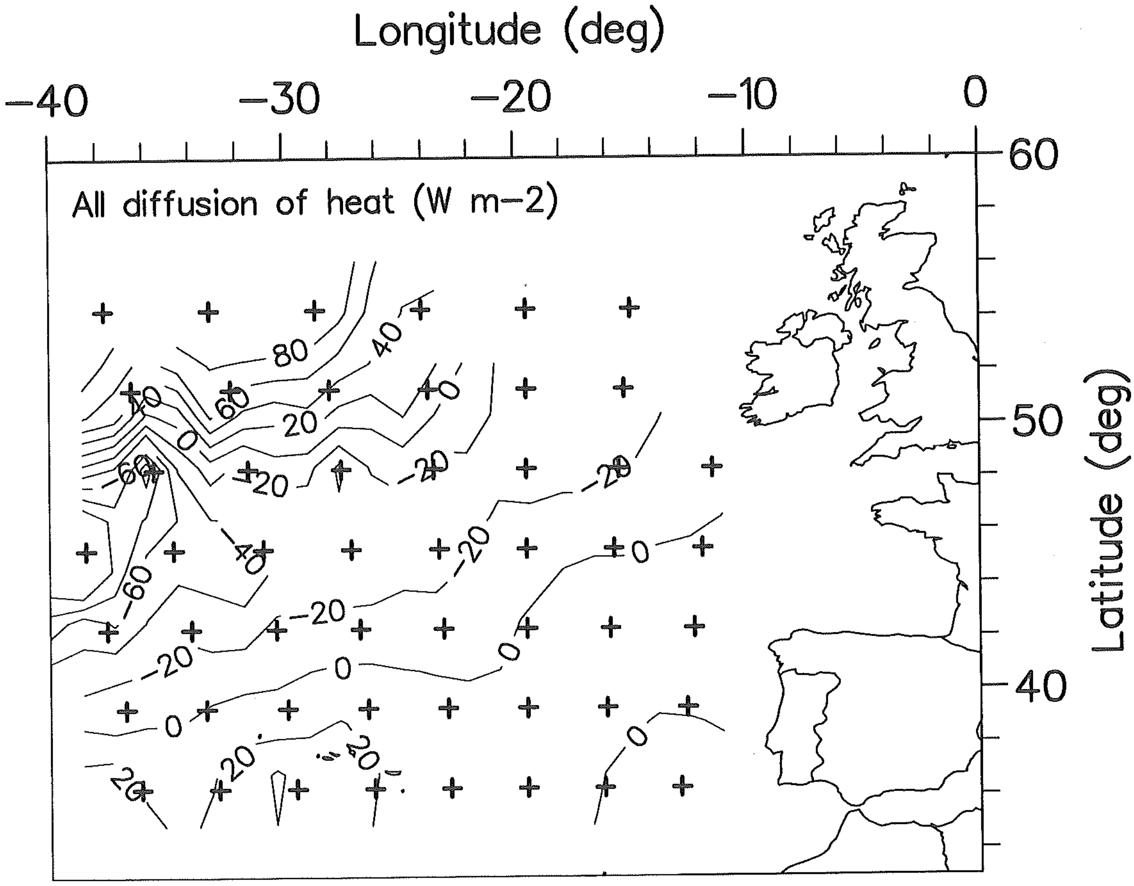

Longitude (deg)
−40
−30
−20
−10
0
60
50
40
Latitude (deg)
All diffusion of heat (W m−2)
80
40
60
20
0
−20
−60
−40

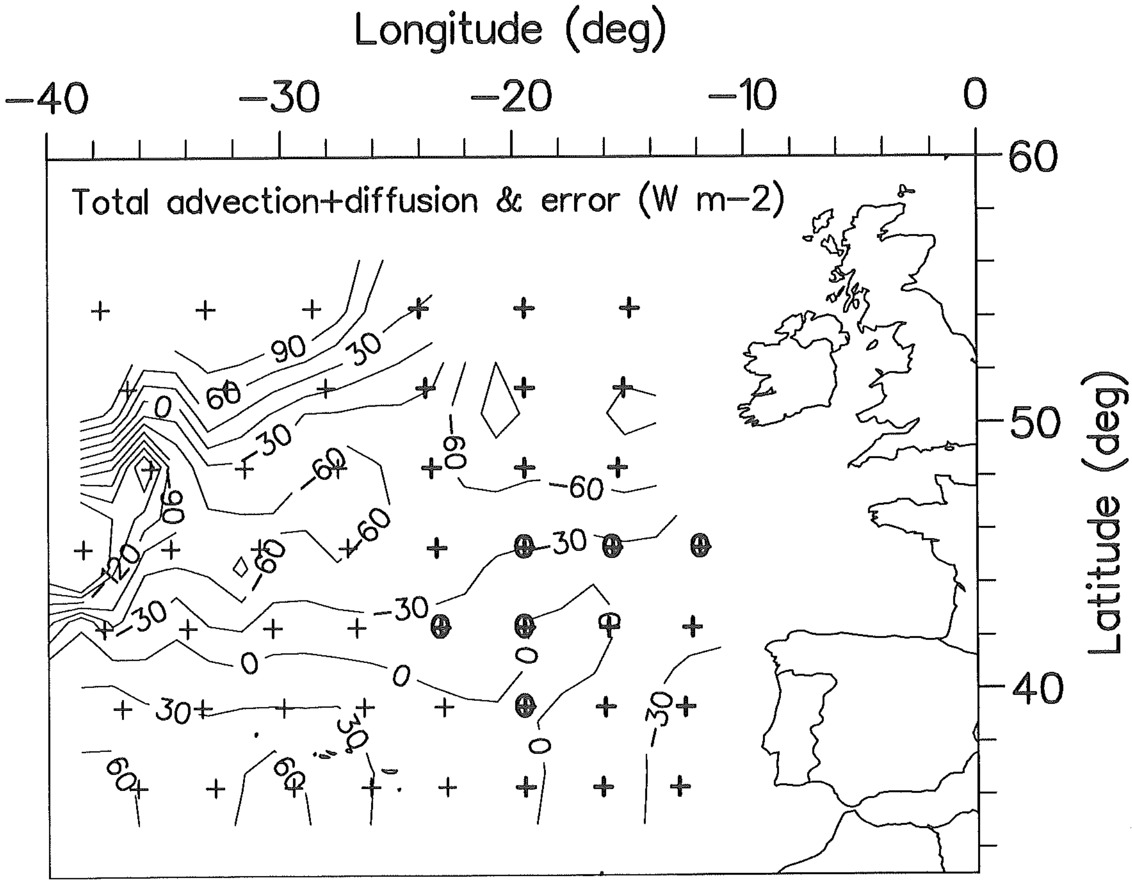
Longitude (deg)
−40
−30
−20
−10
0
60
50
40
Latitude (deg)
Total advection+diffusion & error (W m−2)

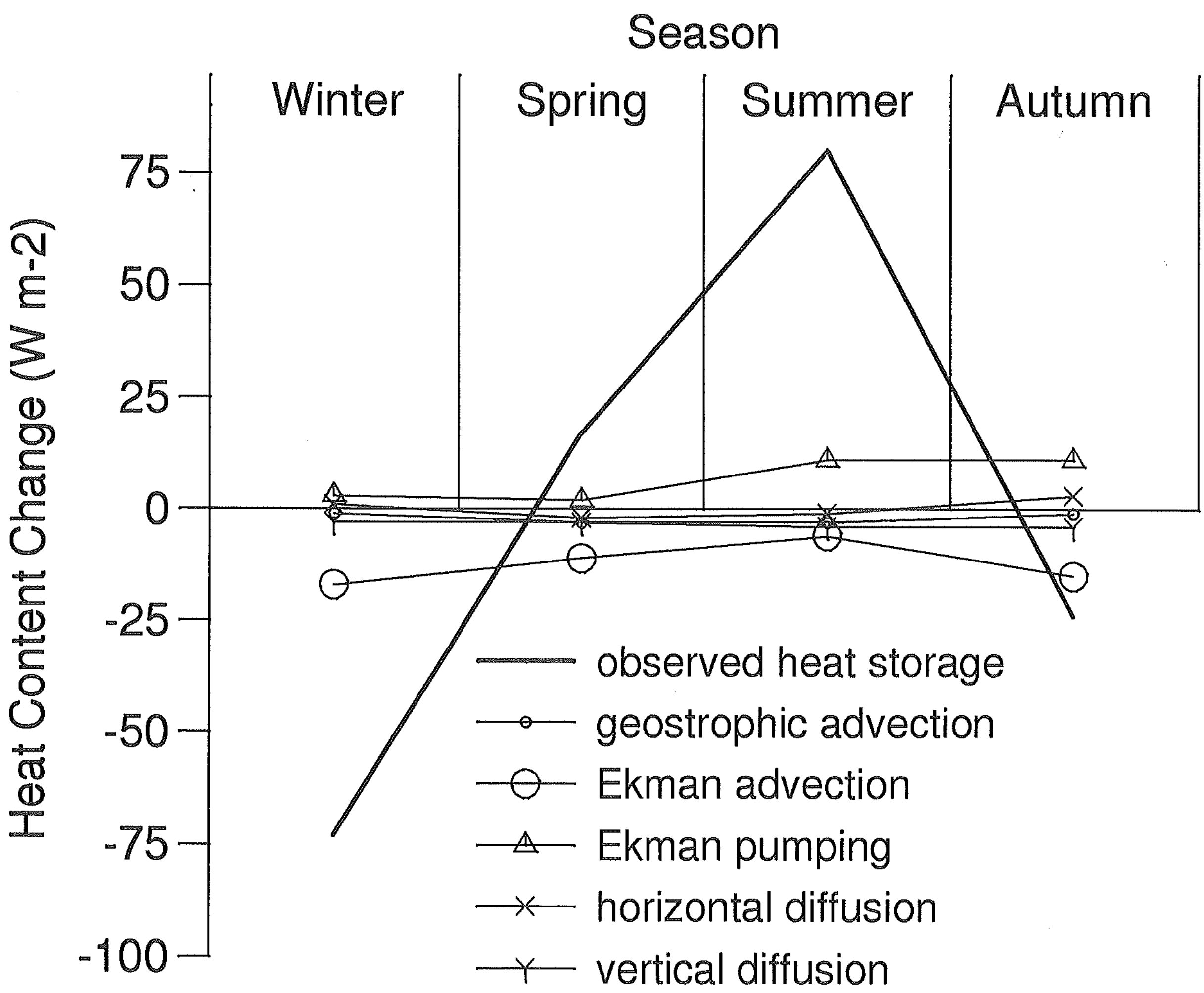

Season
Winter
Spring
Summer
Autumn
75
50
25
0
-25
-50
-75
-100
Heat Content Change (W m-2)
observed heat storage
geostrophic advection
Ekman advection
Ekman pumping
horizontal diffusion
vertical diffusion

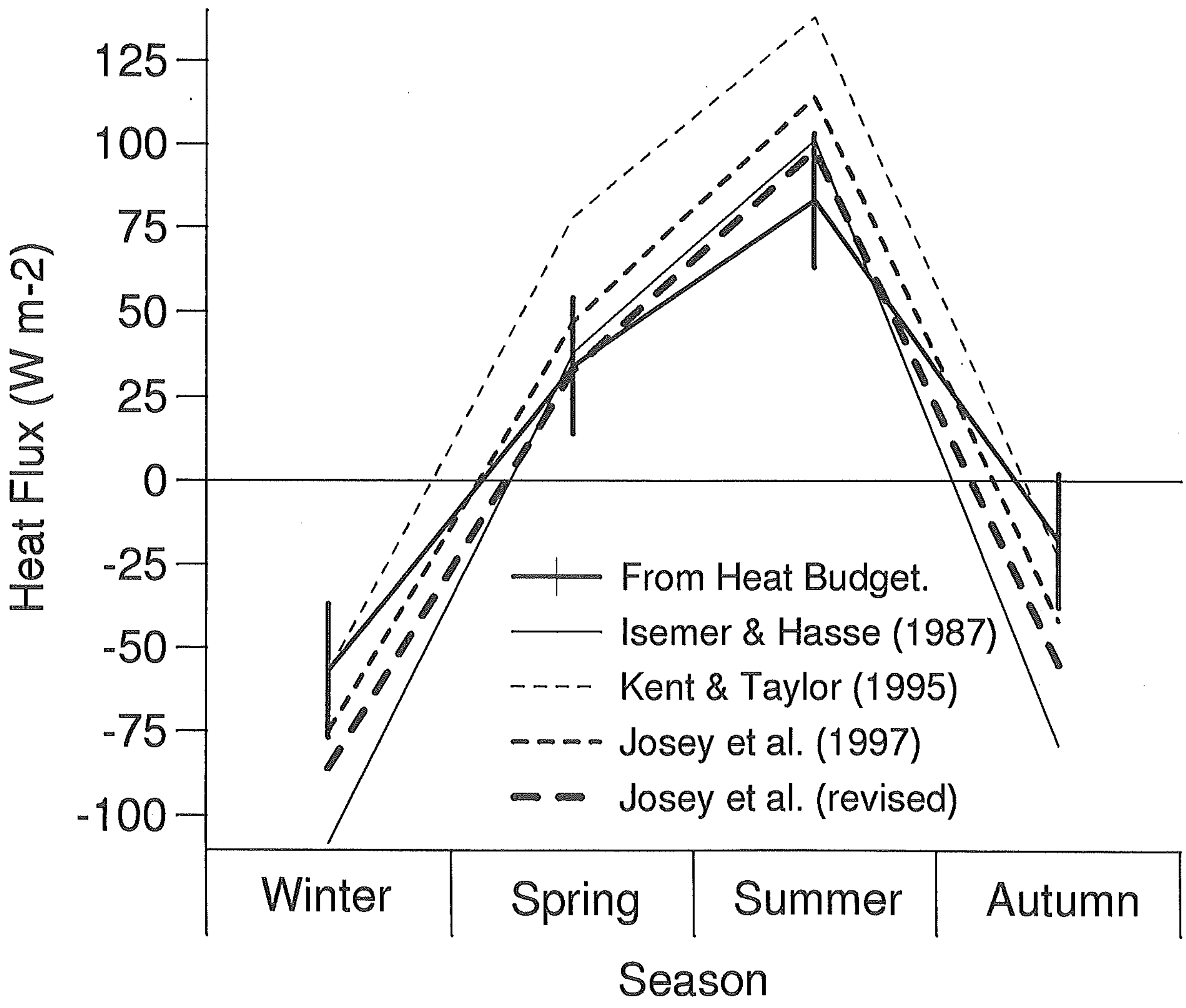

125
100
75
50
25
0
-25
-50
-75
-100
Heat Flux (W m-2)
From Heat Budget.
Isemer & Hasse (1987)
Kent & Taylor (1995)
Josey et al. (1997)
Josey et al. (revised)
Winter
Spring
Summer
Autumn
Season